

TESTING THE RADIATIVELY INEFFICIENT ACCRETION FLOW MODEL FOR SAGITTARIUS A* USING THE SIZE MEASUREMENTS

FENG YUAN,^{1,2} ZHI-QIANG SHEN,^{1,2} AND LEI HUANG^{1,3}

Received 2006 February 12; accepted 2006 March 23; published 2006 April 14

ABSTRACT

Recent radio observations by the Very Long Baseline Array at 7 and 3.5 mm produced the high-resolution images of the compact radio source located at the center of our Galaxy (Sgr A*) and detected its wavelength-dependent intrinsic sizes at the two wavelengths. This provides us with a good chance of testing previously proposed theoretical models for Sgr A*. In this Letter, we calculate the size based on the radiatively inefficient accretion flow (RIAF) model proposed by Yuan, Quataert, & Narayan. We find that after taking into account the scattering of the interstellar electrons, the predicted sizes are consistent with the observations. We further predict an image of Sgr A* at 1.3 mm that can be tested by future observations.

Subject headings: accretion, accretion disks — black hole physics — galaxies: active — Galaxy: center — radiation mechanisms: nonthermal

1. INTRODUCTION

The compact radio source located at the center of our Galaxy (Sgr A*) is perhaps the most intensively studied black hole source to date (see review by Melia & Falcke 2001). Substantial observational results put strict constraints on theoretical models. These models include the spherical accretion model (Melia et al. 2001; Liu & Melia 2002), the pure jet model (Falcke et al. 1993; Falcke & Markoff 2000), the advection-dominated accretion flow (ADAF) model or the radiatively inefficient accretion flow (RIAF) model (Narayan et al. 1995, 1998; Yuan et al. 2003, 2004), and the coupled jet-ADAF model (Yuan et al. 2002). In the present Letter we concentrate on the RIAF model proposed by Yuan et al. (2003, hereafter YQN03).

The YQN03 model explains most of the observations available at that time, including the spectrum from radio to X-ray, the radio polarization, and the flares at both infrared and X-ray wave bands (see YQN03 for detail). After the publication of YQN03, many new observations were conducted. These included using the new spectral variability at millimeter wavelengths (Zhao et al. 2003; Miyazaki et al. 2004; Mauerhan et al. 2005; An et al. 2005), the high angular resolution measurements of the linear polarization at submillimeter wavelengths and its variability with the Submillimeter Array (Marrone et al. 2006), and very high energy emissions from the direction of Sgr A* (*INTEGRAL*: Bélanger et al. 2004; *HESS*: Aharonian et al. 2004; *CANGAROO*: Tsuchiya et al. 2004; *MAGIC*: Albert et al. 2006). Several large multiwavelength campaigns have been performed (e.g., Eckart et al. 2004, 2005; Yusef-Zadeh et al. 2006). Some of the observations mentioned above confirm the YQN03 model (or they can be easily interpreted in the context of this model), while some of the observational results are not so easily understood and thus offer new challenges to the model. In the present Letter we will discuss the size of Sgr A* at radio wavelengths, which has not been discussed in YQN03.

It has long been realized that due to the effect of scattering by the interstellar electrons, the intrinsic size of Sgr A* is only

detectable at short wavelengths (Davies et al. 1976; Lo et al. 1985, 1998; Krichbaum et al. 1997; Bower & Backer 1998). This is because the scattering theory shows that at long wavelengths, the observed image size will be dominated by the scattering and will scale quadratically as a function of wavelength (Narayan & Goodman 1989). At short wavelengths, however, precise measurements of the size of Sgr A* are seriously hampered by calibration uncertainties. Recently, great progress has been made in this respect due to the improvement of the model fitting procedure by means of the closure amplitude. Using the Very Long Baseline Array (VLBA), at 7 mm wavelengths, Bower et al. (2004) successfully measured the size of Sgr A* to be $0.712_{-0.003}^{+0.004}$ mas, and Shen et al. (2005) obtained averaged sizes of 0.724 ± 0.001 and $0.21_{-0.01}^{+0.02}$ mas at 7 and 3.5 mm, respectively. By subtracting in quadrature the scattering size, they obtained an intrinsic size of 0.237 ± 0.02 mas (Bower et al. 2004) or 0.268 ± 0.025 mas (Shen et al. 2005) at 7 mm and 0.126 ± 0.017 mas at 3.5 mm (Shen et al. 2005). Since this new constraint is independent of the other observations, such as the spectrum and variability, it provides us with an independent test to investigate whether or not the RIAF model proposed by YQN03 can account for the observed sizes.

2. RIAF MODEL FOR SGR A*

We first briefly review the RIAF model of YQN03, which can be considered as an updated version of the original ADAF model for Sgr A* (Narayan et al. 1995, 1998). Compared to the ADAF model, the two main developments in the RIAF model are the inclusions of outflow/convection and the possible existence of nonthermal electrons. The former is based on theoretical calculations and numerical simulations (e.g., Stone et al. 1999; Hawley & Balbus 2002). The possible existence of nonthermal electrons is due to acceleration processes such as turbulent acceleration, reconnection, and weak shocks in the accretion flow. We characterize the nonthermal population by p [$n(\gamma) \propto \gamma^{-p}$, where γ is the Lorentz factor] and the parameter η , which is the ratio of the energy in the power-law electrons to that in the thermal electrons. The dynamical quantities describing the accreting plasma, such as the density and temperature, are obtained by globally solving a set of accretion equations, including the conservations of fluxes of mass, momentum, and energy. We assume that the accretion rate is a

¹ Shanghai Astronomical Observatory, Chinese Academy of Sciences, 80 Nandan Road, Shanghai 200030, China; fyuan@shao.ac.cn, zshen@shao.ac.cn, muduri@shao.ac.cn.

² Joint Institute for Galaxy and Cosmology (JOINGC) of SHAO and USTC, 80 Nandan Road, Shanghai 200030, China.

³ Graduate School of Chinese Academy of Sciences, Beijing 100039, China.

function of radius, i.e., $\dot{M} = \dot{M}_0(R/R_{\text{out}})^s$ (e.g., Blandford & Begelman 1999). Here R_{out} is the outer radius of the flow, i.e., the Bondi radius, and \dot{M}_0 is the accretion rate at R_{out} (the Bondi accretion rate, fixed by *Chandra* observations of diffuse gas on $\sim 1''$ scales; Baganoff et al. 2003). The radiative processes we considered include synchrotron emission, bremsstrahlung, and their Comptonization by both thermal and nonthermal electrons. The sum of the self-absorbed synchrotron radiation from the thermal electrons at different radii dominates the radio emission of Sgr A* at ≥ 86 GHz, while the radio emission at ≤ 86 GHz is the sum of the synchrotron emission of both thermal and nonthermal electrons. As we stated in YQN03, there is not much freedom in the choice of parameter values in the RIAF model.

To calculate the intrinsic size of Sgr A* predicted by the RIAF model and compare it with observations, we need to adjust the mass of the black hole. The mass of the black hole adopted in YQN03 is $2.5 \times 10^6 M_\odot$. Recent observations show that the mass should be larger: $M/M_\odot = (3.7 \pm 1.5)$, (3.3 ± 0.6) , and $(4.1 \pm 0.6) \times 10^6$ in Schödel et al. (2002, 2003), and Ghez et al. (2003), respectively. We adopt $M = 4 \times 10^6 M_\odot$. Thus, the model parameters need to be adjusted accordingly to ensure that the adjusted model can fit the spectrum of Sgr A* equally well. The new parameters are $\dot{M}_0 \approx 10^{-6} M_\odot \text{ yr}^{-1}$, $s = 0.25$, $\eta = 0.4\%$, and the fraction of the turbulent energy directly heating electrons $\delta = 0.3$. We note that the values of \dot{M}_0 , s , and η change little, but the value of δ decreases from 0.55 in YQN03 to the present 0.3. This is because the electron temperature needs to decrease a bit to compensate for the increase of flux due to the increase of the mass of the black hole.

3. THE SIZE OF SGR A* PREDICTED BY THE RIAF MODEL

The observed radio morphology of Sgr A* is broadened by the interstellar scattering, which is an elliptical Gaussian distribution along a position angle of $\sim 80^\circ$ with the major- and minor-axis sizes in units of milliarcseconds of $\theta_{\text{scat}}^{\text{maj}} = (1.39 \pm 0.02)\lambda^2$ and $\theta_{\text{scat}}^{\text{min}} = (0.69 \pm 0.06)\lambda^2$, respectively (Shen et al. 2005). The observing wavelength λ is in units of centimeters. To get the intrinsic size of Sgr A*, observers have to subtract the scattering effect from the observed image. Here all the sizes estimated from observations are referred to as the FWHM of the Gaussian profile. This requires that not only the observed apparent image be well characterized by a Gaussian distribution but also the intrinsic intensity profile of the source. However, this may not necessarily be the case. For Sgr A*, we will show that the intrinsic intensity profile emitted by the RIAF can be quite different from the Gaussian distribution. In this case, we are unclear as to the definition of the ‘‘intrinsic size,’’ let alone the comparison between the theoretically predicted size and the observationally derived one. Given this situation, in the present Letter we will not try to calculate the ‘‘intrinsic’’ size of Sgr A*. Rather, we first calculate the intrinsic intensity profile from the RIAF model. Then we take into account the scatter broadening toward the Galactic center to obtain the simulated image. We will directly compare the simulated image with the observed one.

Now let us calculate the specific intensity profile of the radiation from the RIAF. We first assume that the black hole in Sgr A* is nonrotating and that the RIAF is face-on. The effects of the assumptions on the result will be discussed later. We first solve the global solution to obtain the dynamical quantities of the RIAF as stated in § 2. Because the Paczyński & Wiita

(1980) potential is used in our calculation and because the calculation is in the frame of Newtonian mechanics rather than exact general relativity (GR), the calculated radial velocity of the accretion flow very close to the black hole is larger than the speed of light and thus is not physical. As a result, at this region, the density of the accretion flow is smaller, and correspondingly the electron temperature is also lower due to weaker compression. To correct this effect, for simplicity we compare the radial velocity obtained in our calculation with that obtained by Popham & Gammie (1998) in the frame of GR. We found that our radial velocity at $r \lesssim 30$ should be divided by $0.93e^{2.13/r}$, where r is the radius in units of R_g ($\equiv GM/c^2$). As for the electron temperature, following the result in Narayan et al. (1998), a correction factor of $1.4r^{0.097}$ is adopted. The above corrections are of course not precise, but fortunately the result is not sensitive to them, as we will discuss in § 4.

The resulting intrinsic intensity profiles at 3.5 and 7 mm are shown by the red solid lines in Figures 1*b* and 1*f*. Obviously, these two profiles cannot be well represented by a Gaussian distribution. Before we incorporate the electron scattering, however, we take into account the following additional relativistic effects, namely, gravitational redshift, light bending, and Doppler boosting (Jaroszynski & Kurpiewski 1997; Falcke et al. 2000). We implement these effects using our GR ray-tracing code (L. Huang et al. 2006, in preparation). The dashed lines in Figures 1*b* and 1*f* show the resultant intensity profiles after the above GR effects are considered. The original peak of each solid line becomes lower because of the strong gravitational redshift near the black hole. The outward movement of the peak location is due to light bending.

Figures 1*c* and 1*g* show the simulated image after the scattering has been included. The scattering model mentioned at the beginning of this section is adopted. The images are elliptical, consistent with observations. The open circles in Figures 1*d* and 1*h* show the intensity of the simulated image as a function of radius. The smoothness of the profile is the result of the broadening scatter. The solid lines in Figures 1*d* and 1*h* show the Gaussian distributions fitted to the open circles. It can be seen that the intensity profile of the simulated image can be perfectly fitted by a Gaussian distribution, as we stated above. The FWHM values of the simulated images at 7 and 3.5 mm are $0.729^{+0.01}_{-0.009}$ and $0.248^{+0.001}_{-0.002}$ mas, respectively. The simulated size at 7 mm is in good agreement with the observed value by Shen et al. (2005) within the error bars but is slightly larger than the observed size found in Bower et al. (2004); the size at 3.5 mm is a little larger than the observation of Shen et al. (2005). Given that the size of the source may be variable (Bower et al. 2004) and given the uncertainties in our calculations, which we will discuss in § 4, we conclude that the predictions of the YQN03 model are in reasonable agreement with the size measurements.

In the above simulation, the ‘‘input’’ intensity profile for the scattering simulation is the result of considering various effects or corrections. In the following we discuss the effects of these corrections by considering various ‘‘input’’ intensity profiles. The first profile we consider is the one without the GR effect, i.e., the red solid lines in Figures 1*b* and 1*f*. In this case, the FWHM values of the simulated image, after considering electron scattering, are 0.737 and 0.239 mas at 7 and 3.5 mm, respectively. Therefore, the GR effects make the size of Sgr A* slightly larger at 3.5 mm. This is because the strong GR effects make the emission that is very close to the black hole weaker, while the emission at large radii almost remain unchanged. But at 7 mm, since the scattering effect is much stronger (4 times) than at

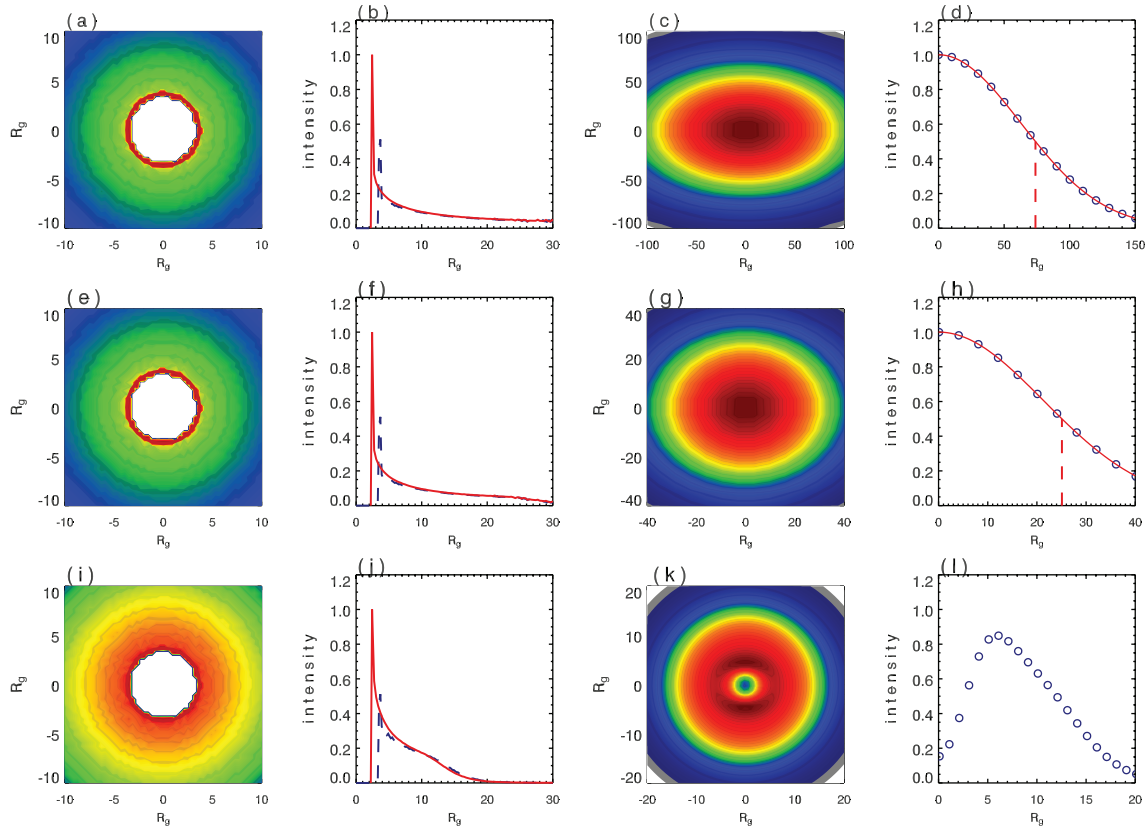


FIG. 1.—Images and sizes of Sgr A* at 7 (*top panels*), 3.5 (*middle panels*), and 1.3 mm (*bottom panels*). At each row of panels, the first panel shows the “input” intensity distribution. The solid line in the second panel is the intensity profile calculated from the RIAF model, and the dashed line is the intensity profile after the GR effects are taken into account using the ray-tracing method. The third panel shows the simulated image after the interstellar scattering is taken into account. The open circles in the fourth panel show the intensity profile of the simulated image, and the solid line shows the Gaussian distribution fitted to the circles. The vertical dashed line shows the location of the FWHM. At 1.3 mm, the simulated profile cannot be fitted by a Gaussian distribution, and thus no FWHM is indicated.

3.5 mm, the emission at both the small and large radii in the scattered intensity profile becomes weaker due to the GR effects. The total effect is that the size becomes smaller at 7 mm. We have confirmed our interpretation by simulating the image at a longer wavelength (i.e., 14 mm). The second profile we consider is based on the last profiles (i.e., without considering GR effects), with the only difference being that we now only consider the emission of thermal electrons in calculating the intrinsic intensity profiles. The FWHM values of the simulated image in this case are 0.724 and 0.228 mas at 7 and 3.5 mm, respectively. Therefore, the inclusion of the nonthermal electrons in the RIAF makes the size of Sgr A* at 7 and 3.5 mm larger. This is because the intensity profile from the nonthermal electrons is flatter than that from the thermal electrons. The last input intensity profile we consider is based on the second profile above (i.e., without considering nonthermal electrons), but with the difference being that the profiles of the density and electron temperature are directly obtained from the global solution of the RIAF and that no relativistic corrections to the profiles of the density and temperature are adopted. In this case, the FWHM values of the simulated image are 0.727 and 0.238 mas at 7 and 3.5 mm, respectively. Therefore, the inclusion of relativistic corrections to the profiles of the density and electron temperature makes the size of Sgr A* smaller. This is because the corrections make the emission at the innermost region of the RIAF stronger.

We also calculated the simulated size of Sgr A* at 1.35 cm, which is $2.67^{+0.04}_{-0.03}$ mas. This result is consistent with the ob-

served size of $2.635^{+0.037}_{-0.024}$ mas by Bower et al. (2004) and is slightly larger than the size of $2.53^{+0.06}_{-0.05}$ mas by Shen et al. (2005). Finally, we try to predict an observed image of Sgr A* at a shorter wavelength (i.e., 1.3 mm). The red solid line in Figure 1j shows the calculated intensity profile, and the dashed line is the profile after the GR effects are taken into account using the ray-tracing method. The simulated image at 1.3 mm, after considering the electron scattering, is shown in Figure 1k, and its intensity profile is shown in Figure 1l. Different from the cases of 7 mm (Fig. 1d) and 3.5 mm (Fig. 1h), however, the simulated intensity profile can no longer be reasonably fitted by a Gaussian distribution (see also Fig. 1 in Falcke et al. 2000). This indicates that the ratio between the intrinsic size and the scattering size must be larger at 1.3 mm than that at 3.5 mm, where the two sizes are comparable. And as a result, the non-Gaussian distribution of the intrinsic intensity distribution significantly modulates the observed image. This prediction can be tested by future VLBI observations.

4. SUMMARY AND DISCUSSION

The recent VLBA observations (Shen et al. 2005; Bower et al. 2004) produced high-resolution images of Sgr A* at wavelengths of 3.5 and 7 mm. The measured sizes provide us with a good chance of testing theoretical models. In this Letter we investigate whether the RIAF model presented in YQN03 can account for these new observations. We calculate the intrinsic

intensity profile of the RIAF, taking into account the relativistic corrections such as light bending and gravitational redshift. Because the intrinsic intensity profile produced by the YQN03 model cannot be represented by a Gaussian distribution (see the solid lines in Figs. 1*b* and 1*f*), we simulate the image by considering the interstellar scattering. The results are shown in Figures 1*d* and 1*h*. The intensity profile of such an image can be fitted by a Gaussian distribution, and we thus obtain its FWHM value and compare it directly with the observations (Figs. 1*d* and 1*h*). The predicted sizes of Sgr A* by the RIAF model of YQN03 at 7 and 3.5 mm are $0.729^{+0.01}_{-0.009}$ and $0.248^{+0.001}_{-0.002}$ mas, respectively, which are in reasonable agreement with observations considering the uncertainties of the calculations. We further predict an image of Sgr A* at 1.3 mm (Figs. 1*k* and 1*l*) that can be tested by future observations.

In our calculations, we assume a face-on RIAF and a non-rotating black hole. If the RIAF is not face-on, the result will be more complicated, depending on the angle between our line of sight and the rotation axis of the RIAF, and the angle between the major axis of the scattering screen and the rotation axis of the RIAF. Therefore, a quantitative estimation of the size in this case is difficult, but given the geometry of the RIAF, we speculate that the results should be similar, even at the extreme case of an edge-on RIAF. If the black hole is rapidly rotating, however, the accretion flow will extend farther inward compared to the case of a nonrotating Schwarzschild hole; thus, the peak in the intensity profile (see Figs. 1*b* and 1*f*) will move to smaller radii, and its amplitude will become higher. This will result in a somewhat smaller size of Sgr A*. Given that the predicted sizes at both 3.5 and 7 mm by the RIAF model around a Schwarzschild black hole are larger than observations, our calculations thus suggest that the black hole in Sgr A* may

be rapidly rotating. The exact prediction of the angular momentum of the black hole needs fully self-consistent radiation-hydrodynamics calculations to both the dynamics and the radiation of the RIAF in the Kerr geometry, which is beyond the scope of the present Letter.

Finally, we briefly discuss the constraint of the observed size of Sgr A* on the other two models of Sgr A*, namely, the jet model of Falcke & Markoff (2000) and the coupled jet-ADAF model of Yuan et al. (2002). One main difference between these two models associated with the present Letter is that in the former, the radio emission above ~ 86 GHz is produced by the nozzle of the jet, while in the latter, the contribution of the ADAF is significant. Falcke & Markoff (2000) calculated the size of Sgr A*. The predicted sizes of Sgr A* at 3.5 mm by the nozzle and the jet components are ~ 0.04 and 0.16 mas, respectively. Since in this model the emission at 3.5 mm is dominated by the nozzle rather than the jet, the predicted size might be ≥ 0.04 mas, much smaller than the observed value. Numerical calculations are required to confirm this speculation. On the other hand, in the jet-ADAF model, the contribution of the emission from the ADAF can dominate over that from the jet under suitable parameters. In this case, the predicted size of Sgr A* will be consistent with the observations, as we show in the present Letter. Of course, the ADAF component in that model needs to be replaced by an RIAF, i.e., considering the outflow/convection. In that case, the main difference between the jet-ADAF model and the RIAF model is the origin of the radio emission below ~ 86 GHz.

This work was supported in part by the One-Hundred-Talent Program and the National Natural Science Foundation of China (grants 10543003 and 10573029).

REFERENCES

- Aharonian, F., et al. 2004, *A&A*, 425, L13
 Albert, J., et al. 2006, *ApJ*, 638, L101
 An, T., Goss, W. M., Zhao, J.-H., Hong, X. Y., Roy, S., Rao, A. P., & Shen, Z.-Q. 2005, *ApJ*, 634, L49
 Baganoff, F. K., et al. 2003, *ApJ*, 591, 891
 Bélanger, G., et al. 2004, *ApJ*, 601, L163
 Blandford, R. D., & Begelman, M. C. 1999, *MNRAS*, 303, L1
 Bower, G. C., & Backer, D. C. 1998, *ApJ*, 496, L97
 Bower, G. C., Falcke, H., Herrnstein, R. M., Zhao, J.-H., Goss, W. M., & Backer, D. C. 2004, *Science*, 304, 704
 Davies, R. D., Walsh, D., & Booth, R. S. 1976, *MNRAS*, 177, 319
 Eckart, A., et al. 2004, *A&A*, 427, 1
 ———. 2005, *A&A*, submitted (astro-ph/0512440)
 Falcke, H., Mannheim, K., & Biermann, P. L. 1993, *A&A*, 278, L1
 Falcke, H., & Markoff, S. 2000, *A&A*, 362, 113
 Falcke, H., Melia, F., & Agol, E. 2000, *ApJ*, 528, L13
 Ghez, A. M., et al. 2003, *ApJ*, 586, L127
 Hawley, J. F., & Balbus, S. A. 2002, *ApJ*, 573, 738
 Jaroszynski, M., & Kurpiewski, A. 1997, *A&A*, 326, 419
 Krichbaum, T. P., et al. 1997, *A&A*, 323, L17
 Liu, S., & Melia, F. 2002, *ApJ*, 566, L77
 Lo, K. Y., Backer, D. C., Ekers, R. D., Kellermann, K. I., Reid, M., & Moran, J. M. 1985, *Nature*, 315, 124
 Lo, K. Y., Shen, Z.-Q., Zhao, J.-H., & Ho, P. T. P. 1998, *ApJ*, 508, L61
 Marrone, D. P., Moran, J. M., Zhao, J.-H., & Rao, R. 2006, *ApJ*, 640, 308
 Mauerhan, J. C., Morris, M., Walter, F., & Baganoff, F. K. 2005, *ApJ*, 623, L25
 Melia, F., & Falcke, H. 2001, *ARA&A*, 39, 309
 Melia, F., Liu, S., & Coker, R. 2001, *ApJ*, 553, 146
 Miyazaki, A., Tsutsumi, T., & Tsuboi, M. 2004, *ApJ*, 611, L97
 Narayan, R., & Goodman, J. 1989, *MNRAS*, 238, 963
 Narayan, R., Mahadevan, R., Grindlay, J. E., Popham, R. G., & Gammie, C. 1998, *ApJ*, 492, 554
 Narayan, R., Yi, I., & Mahadevan, R. 1995, *Nature*, 374, 623
 Paczyński, B., & Wiita, P. J. 1980, *A&A*, 88, 23
 Popham, R., & Gammie, C. F. 1998, *ApJ*, 504, 419
 Schödel, R., Ott, T., Genzel, R., Eckart, A., Mouawad, N., & Alexander, T. 2003, *ApJ*, 596, 1015
 Schödel, R., et al. 2002, *Nature*, 419, 694
 Shen, Z.-Q., Lo, K. Y., Liang, M.-C., Ho, P. T. P., & Zhao, J.-H. 2005, *Nature*, 438, 62
 Stone, J., Pringle, J., & Begelman, M. 1999, *MNRAS*, 310, 1002
 Tsuchiya, K., et al. 2004, *ApJ*, 606, L115
 Yuan, F., Markoff, S., & Falcke, H. 2002, *A&A*, 383, 854
 Yuan, F., Quataert, E., & Narayan, R. 2003, *ApJ*, 598, 301 (YQN03)
 ———. 2004, *ApJ*, 606, 894
 Yusef-Zadeh, F., et al. 2006, *ApJ*, in press (astro-ph/0510787)
 Zhao, J.-H., Young, K. H., Herrnstein, R. M., Ho, P. T. P., Tsutsumi, T., Lo, K. Y., Goss, M. W., & Bower, G. C. 2003, *ApJ*, 586, L29